UNIVERSITY OF BIRMINGHAM
University of Birmingham Research at Birmingham

Millimeter-Wave High Gain Frequency-Scanned Antenna Based on Waveguide Continuous Transverse Stubs

You, Yang; Lu, Yunlong; You, Qingchun; Wang, Yi; Huang, Jifu; Lancaster, Michael

DOI:
10.1109/TAP.2018.2863298

License:
None: All rights reserved

Document Version
Peer reviewed version

Citation for published version (Harvard):
You, Y, Lu, Y, You, Q, Wang, Y, Huang, J & Lancaster, M 2018, 'Millimeter-Wave High Gain Frequency-Scanned Antenna Based on Waveguide Continuous Transverse Stubs', *IEEE Transactions on Antennas and Propagation*. https://doi.org/10.1109/TAP.2018.2863298

Link to publication on Research at Birmingham portal

Publisher Rights Statement:
© Copyright 2018 IEEE.

Checked 26/7/18.

General rights
Unless a licence is specified above, all rights (including copyright and moral rights) in this document are retained by the authors and/or the copyright holders. The express permission of the copyright holder must be obtained for any use of this material other than for purposes permitted by law.

•Users may freely distribute the URL that is used to identify this publication.
•Users may download and/or print one copy of the publication from the University of Birmingham research portal for the purpose of private study or non-commercial research.
•User may use extracts from the document in line with the concept of 'fair dealing' under the Copyright, Designs and Patents Act 1988 (?)
•Users may not further distribute the material nor use it for the purposes of commercial gain.

Where a licence is displayed above, please note the terms and conditions of the licence govern your use of this document.

When citing, please reference the published version.

Take down policy
While the University of Birmingham exercises care and attention in making items available there are rare occasions when an item has been uploaded in error or has been deemed to be commercially or otherwise sensitive.

If you believe that this is the case for this document, please contact UBIRA@lists.bham.ac.uk providing details and we will remove access to the work immediately and investigate.

Download date: 25. Apr. 2024

Millimeter-Wave High Gain Frequency-Scanned Antenna Based on Waveguide Continuous Transverse Stubs

Yang You, Yunlong Lu, Qingchun You, Yi Wang, Jifu Huang, and Michael J. Lancaster

***Abstract*—A millimeter-wave frequency-scanned antenna (FSA) based on continuous transverse stubs (CTSs) for beam steering applications is presented in this communication. The waveguide CTS radiation slots are fed by a wideband quasi-TEM linear source generator (LSG). To increase the scanning angle, a non-uniform slow-wave structure is employed underneath the radiation slots to control the amplitude and phase distributions. The LSG is constructed of a parallel-plate waveguide (PPW) excited by a modified three-stage 1-to-8 power divider, generating high quality quasi-TEM wave over a wide frequency band. The beam direction is tunable with varying frequency. To validate the design, a prototype array at Ka-band is designed, fabricated and measured. Excellent agreement is achieved between simulations and measurements. The measured results show that the proposed array has an impedance bandwidth from 26 to 42 GHz (47%). The peak gain is 22.9-29.2 dBi and the radiation angle can be scanned from −56.2° to −2.2°. Over the entire frequency band, the first sidelobe is suppressed to below −12.6 dB.**

***Index Terms*—Frequency scanned antenna, millimeter wave antenna, continuous transverse stub (CTS), high gain antenna, quasi-TEM linear source generator.**

I. Introduction

Millimeter-wave (MMW) antenna arrays with beam steering capability are highly desired in many applications such as radar, imaging and high-speed communications [1]-[3]. There are several established solutions to realize such high performance antenna arrays with high beam-pointing precision. Mechanical scanning antenna arrays are commonly used in the field. But mechanical scanning suffers from reliability issues as well as slow scanning speed [4]-[6]. In contrast, electrical scanning is faster and more flexible [7]-[9]. However, the use of phase shifters in the feed network makes phased arrays complex and expensive. A frequency scanning antenna (FSA) is an alternative beam steering technology. Compared with the phase scanning technology, frequency-scanning features lower hardware cost and circuit complexity. It is also much faster than mechanical scanning.

Various FSAs have been demonstrated, such as E-shaped leaky-wave arrays [10], slot-coupled patch arrays [11], [12] and metamaterial loaded printed FSAs [13]. Most of these FSAs were based on printed circuit board (PCB) technologies. Their losses and fabrication tolerance prevent them from scaling up to MMW region.

This work was supported partly by National Natural Science Foundation of China under Projects 61631012 and 61571251, in part by Natural Science Foundation of Zhejiang LQ17F010002 and K.C. Wong Magna Fund in Ningbo University. The work of Yi Wang was supported by UK EPSRC under Contract EP/M013529/1. (*Corresponding author*: Yunlong Lu.)

Y You, Q. You, Y. Lu, and J. Huang are with the Faculty of Electrical Engineering and Computer Science, Ningbo University, Ningbo, Zhejiang, 315211, China (e-mail: luyunlong@nbu.edu.cn).

Y. Lu is also with State Key Laboratory of Millimeter Waves, Southeast University, Nanjing 210096, China.

Y. Wang and M. J. Lancaster are with the Department of Electronic, Electrical and Systems Engineering, University of Birmingham, B15 2TT, United Kingdom (e-mail: y.wang.1@bham.ac.uk).

Color versions of one or more of the figures in this communication are available online at http://ieeexplore.ieee.org.

Digital Object Identifier 10.1109/TAP.2016.xxx

At MMW frequencies, slotted waveguide (SW) has been a popular structure to achieve high-performance FSAs. A 2-D FSA based on slotted waveguides, fed by a phase shifting network, was demonstrated in [14]. The antenna was capable of scanning a 60° × 20° region and the achieved fractional bandwidth was 25% (240 - 310 GHz). A W-band FSA using slotted micro-coaxial lines was reported in [15]. The array achieved a 30° scanning angle over an operating bandwidth of 87 - 102 GHz.

Continuous transverse stub (CTS) antenna arrays have long been considered a promising technology for advanced antenna systems at MMW frequencies [16], [17]. In the past few years, CTS technology has been applied to FSAs. In [18], a CPW-CTS antenna array with metamaterial-based phase shifters was proposed. A scanning angle of 58° - 124° with a peak gain of 9.7 dBi was achieved. A 16-element X/Ku-band CTS FSA based on substrate integrated waveguides (SIWs) with a scanning-angle of 52.2° to -16.8° and peak gain of 18.1 dBi was proposed in [19]. In [20], SIW technology was also used, achieving a scanning range from −43° to 3° over the frequency range of 27 - 36 GHz (28.5%) and a peak gain of 16.9 dBi. Still, all abovementioned CTS FSAs are based on PCB technologies. The design of a high-performance waveguide-CTS-based FSA with low-profile, high gain and wide scanning range remains a big challenge.

In this paper, a novel CTS FSA is proposed using waveguide technology for MMW applications. Seventeen CTS radiation slots are used to achieve a high gain of over 22.9 dBi. The main novelties and features of the design are a non-uniform slow-wave structure and a wideband linear source generator (LSG). Different from [23] where a uniform slow-wave structure was reported, a sloped slow-wave structure is used to optimize the amplitude and phase distribution across the radiation slots, which controls the scanning angle and increases peak gain. Very recently, [24] reported an analysis and simulation of a similar non-uniform slow-wave structure. However, the design assumed an ideal plane-wave excitation port without a circuit implementation. So it was incomplete and not experimentally verified. This paper presents a complete treatment of the slow-wave structure and experimental verification. As for the linear source generator, our design employs a multiple-port excited parallel-plate waveguide (PPW) cascaded with a PPW bend based on waveguide, which is different from [23] and exhibits much wider bandwidth. This not only simplifies the structure but also, more importantly, provides a much wider antenna operating bandwidth (47% in this work versus about 13% in [23]). The unique combination of the above features renders this work a high-performance waveguide-based CTS with very competitive frequency scanning capability.

II. Antenna Design and Analysis

The proposed waveguide-CTS-based FSA is shown in Fig. 1(a). It consists of three layered blocks: the waveguide feed structure in the bottom layer (M3) and the radiation and slow-wave structure in the layers M1-M2. The feed structure contains a transition from a stand-

0018-926X © 2017 IEEE. Personal use is permitted, but republication/redistribution requires IEEE permission.
See http://www.ieee.org/publications_standards/publications/rights/index.html for more information.

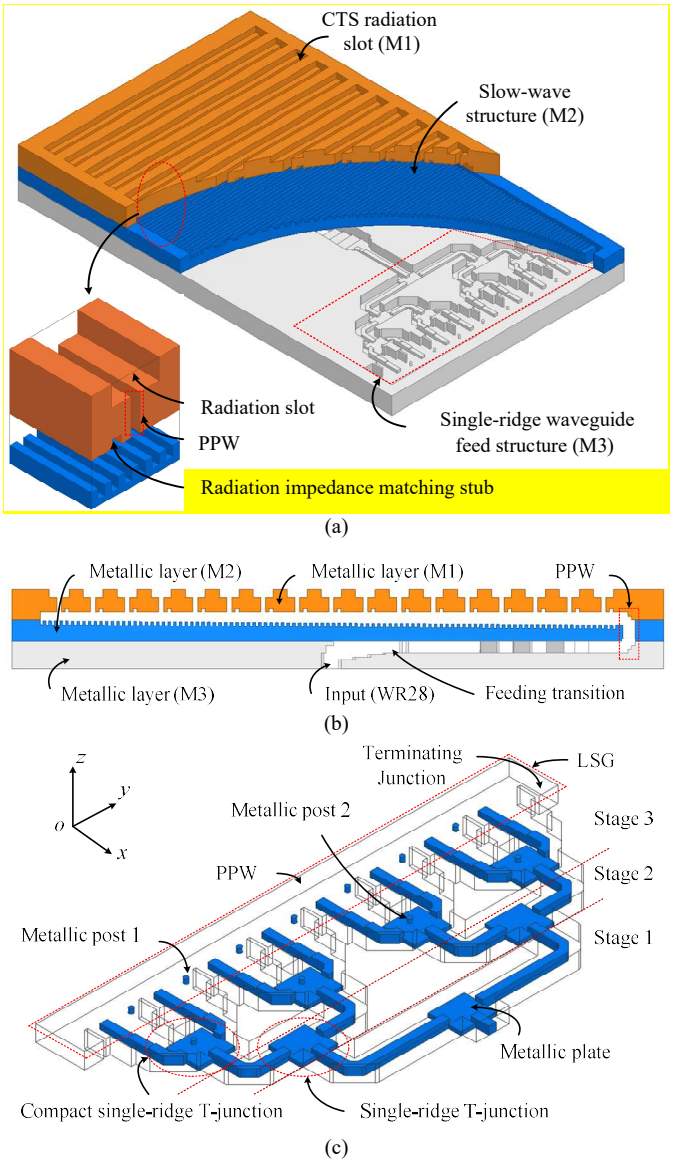

Fig. 1. Configuration of the frequency-scanned CTS array. (a) Perspective view; (b) Side view; (c) Partial view of the feed structure.

ard input waveguide (WR28) to a single-ridge waveguide followed by a 1-to-8 ridge-waveguide power divider. This can be seen in Fig. 1(b) and (c). The radiation parts include 17 CTS radiation elements in Layer M1 and a non-uniform slow-wave structure underneath in Layer M2. As shown in Fig. 1(b), the radiation part and the feed structure are connected through a PPW. This also works as the LSG of the quasi-TEM wave to excite the radiation slots. More design details and analysis are given below. All the simulations are carried out with Ansoft HFSS.

A. CTS radiation slots and non-uniform slow-wave structure

The 17 CTS radiation elements are serially excited by the quasi-TEM wave from the LSG. An enlarged view of one radiating element of the FSA is shown in Fig. 1(a). Each element contains a stepped-width radiation slot and an impedance matching stub. Widths of the radiation slots are varied to control the power coupled from the non-uniform slow-wave structure and to enhance the operating bandwidth [21]. The stubs help with impedance matching and reduce the reflection of the quasi-TEM wave from the radiation

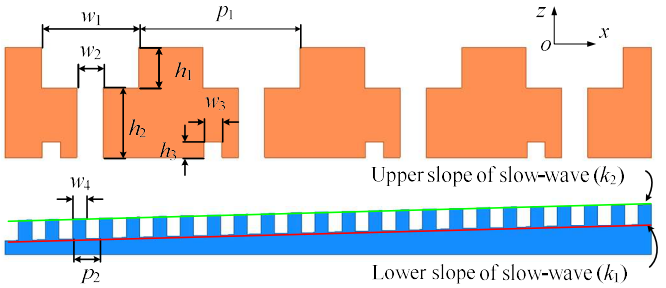

Fig. 2. Partial view of the CTS radiation slots and the non-uniform slow-wave structure.

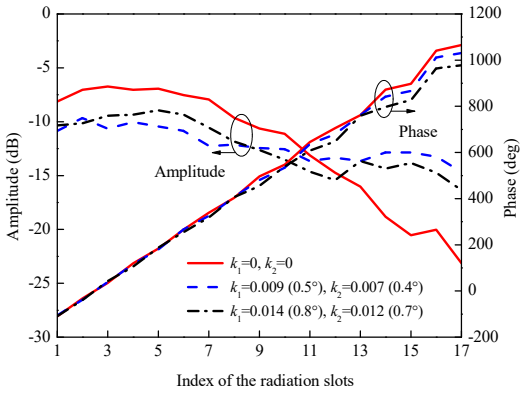

Fig. 3. The amplitude and phase characteristics under different combinations of slopes k_1 and k_2 of the non-uniform slow-wave structure when all other parameters in Fig. 2 are kept the same and given in the texts.

slots [22].

The sloped non-uniform slow-wave structure in layer M2 has two functions: (i) It shortens the wavelength in the air-filled PPW [23]. This effectively enlarges the phase difference between the adjacent radiation slots, resulting in a wider scanning angle than the FSA without the slow-wave structure; (ii) It optimizes the amplitude and phase distributions at the radiation slots for beam scanning, as will be discussed in more details later. In this design, the antenna is designed to operate over a broad band from 26 to 42 GHz. The period of the radiation slot p_1 (Fig. 2) is chosen to be the guided wavelength (λ_{gmin}) of the slow-wave structure at the highest operating frequency f_H. That is 6.2 mm. As a result, the overall length of the FSA antenna is 105 mm, and its width is determined by the width of the LSG (which is 63 mm as will be discussed later).

With this value of p_1, it is naturally less than the free-space wavelength (7.1 mm at 42 GHz in this case~~),~~. ~~the~~ The grating lobes have therefore been avoided for all the concerned frequencies. At the same time, the equal-phase of the excitation for all the radiation slots at f_H can be achieved. So, the main beam at f_H (42 GHz) is pointed to the z-axis (Fig. 1). In order to satisfy this, the amplitudes of the excitation signal at the radiation slots should be equal, and the phase increment between them constant at f_H. This is realized by carefully controlling the upper and lower slope of the slow-wave structure as shown in Fig. 2. Here k_1 and k_2 are defined as the tangent values of the tilt angle between the slow-wave structure and the horizontal plane (x-axis). The optimized parameters of the radiation slots and the slow-wave structure in Fig. 2 are: w_1 = 3.6 mm, h_1 = 1.54 mm, w_2 = 0.9 mm, h_2 = 2.7 mm, w_3 = 0.68 mm, h_3 = 0.6 mm, w_4 = 0.5 mm, p_1 = 6.2 mm, and p_2 = 1 mm. Fig. 3 shows the amplitude and phase characteristics under different combinations of k_1 and k_2 at 42 GHz. Note that when k_1 = 0 and k_2 = 0, it represents a uniform slow-wave structure and the imbalance is significant. When k_1 = 0.009 (0.5° tilt

angle) and k_2 = 0.007 (0.4° tilt angle), the amplitudes and the phases across the slots become sufficiently equal. When the operating frequency varies, the phases of the quasi-TEM wave between adjacent radiation slots are no longer equal. This results in the change of the beam direction.

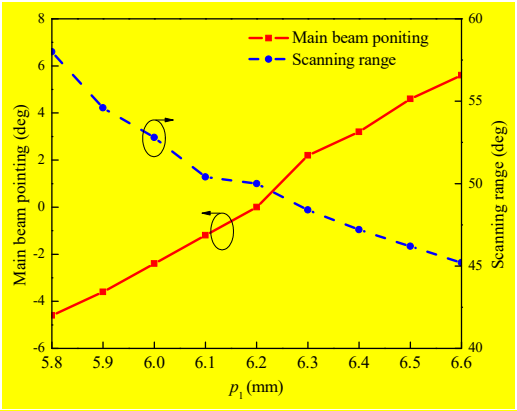

Fig. 4. Effect of p_1 on the scanning ranges and main beam pointing at 42 GHz.

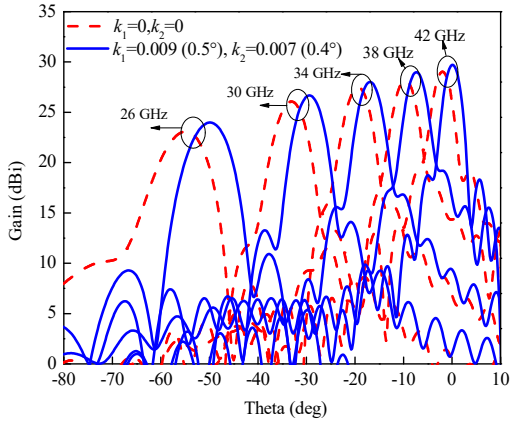

Fig. 5. Comparison of the simulated frequency scanning with a uniform and a non-uniform slow-wave structure.

Based on the non-uniform slow-wave structure with equal amplitude and phase distributions at 42 GHz, the frequency scanning performance under different values of p_1 is investigated as shown in Fig. 4. It can be seen that the main beam pointing at 42 GHz shifts from 5.7° to -4.8° with p_1 decreasing from 6.6 mm to 5.8 mm. When p_1= 6.2 mm, the main beam points to θ = 0° as designed. Besides, the scanning range increases ~~correspondingly~~ with decreasing p_1 ~~decreases~~. Fig. 5 compares the simulated frequency scanning between a uniform and a non-uniform slow-wave structure. With the non-uniform slow-wave structure, the beam is scanned from 0° to −50° within the frequency range of 26-42 GHz. The corresponding peak gain decreases from 29.7 to 23.7 dBi. With a uniform slow-wave structure, the main beams are slightly shifted by 2° to 5°. The peak gain is reduced by just over 1 dB to 28.7 dBi at 42 GHz and 22.6 dBi at 26 GHz. This shows the advantage of the non-uniform slow-wave features

B. Linear source generator

The LSG is designed to generate the high-quality quasi-TEM wave which excites the CTS radiation slots. The proposed LSG is constructed of a PPW with multiple-port excitation, as shown in Fig. 1(c). Fig. 6 is the top view of the LSG. Its total width is determined by the number of the excitation ports and the separation d_1 between them. In this work, eight ports are used. When excited, the TE_{10} waves in the single-ridge waveguides are combined into a quasi-TEM wave in the PPW. To improve the amplitude balance of the quasi-TEM wave, a row of inductive metallic posts are loaded between the ridges to reduce the mutual interferences between adjacent ports. In addition, two $\lambda_0/4$ (λ_0 is the free space wavelength at the center operating frequency) terminating offsets are added at both ends of the PPW to suppress the reflections [25].

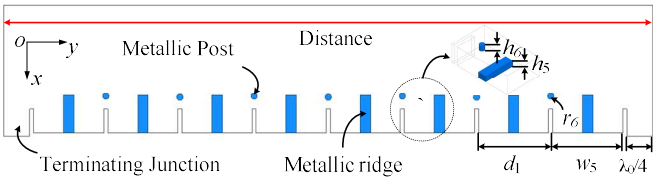

Fig. 6. Top view of the LSG.

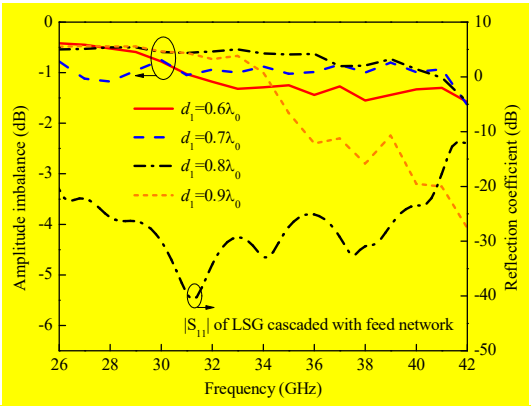

Fig. 7. Simulated E_x-field amplitude imbalance of the quasi TEM wave in the PPW along the y-axis with different inter-element spacing d_1, as well as the simulated reflection coefficient of the LSG.

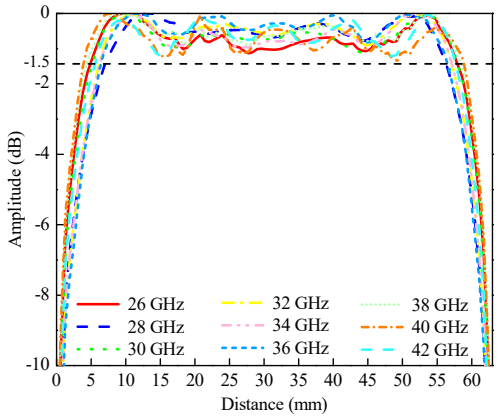

Fig. 8. E_x-field amplitude distribution along the y-axis of the quasi-TEM wave in the LSG over the frequency band of 26-42 GHz.

The amplitude distribution of the quasi-TEM wave along the PPW, excited by the eight waveguide ports with identical phases, has been optimized to achieve a minimum fluctuation in amplitude. This is mainly done by adjusting d_1. The simulated amplitude imbalances (defined as the maximum amplitude fluctuation of the E_x-field in the PPW) as a function of d_1 and frequency are shown in Fig. 7. When d_1 is less than 0.8λ_0, the amplitude fluctuation along the y-axis is within 1.5 dB over 26 - 42 GHz. Since a large inter-element spacing facilitates fabrication, d_1 is chosen to be 0.8λ_0 (7.2 mm) in the final design and therefore the width of LSG becomes 63 mm. The

optimized parameters of the LSG are: $w_5 = 6.8$ mm, $h_5 = 0.7$ mm, $r_6 = 0.3$ mm, and $h_6 = 0.6$ mm. The E_x-field distribution at different frequencies along the y-axis in the PPW (as indicated in Fig. 6) is shown in Fig. 8. It is evident that the amplitude fluctuation is kept under 1.5 dB across the whole operating band. The impedance bandwidth of the optimized LSG cascaded with feed network (to be discussed in the later part) is also shown in Fig. 7. The 20-dB impedance bandwidth is ~~covered~~ from 26 GHz - 40.8 GHz (44.3%) ~~and~~ which indicates a wideband characteristic.

C. Feed network

A 1-to-8 power divider is employed to feed the LSG, as shown in Fig. 1(c). It consists of three stages of T-junctions. To reduce the size of the air-waveguide structure and enhance bandwidth, the whole feed network is designed using single-ridge waveguides.

It is noted that the T-junction at the third stage is modified to accommodate the chosen d_1. Fig. 9 shows the normal and the modified single-ridge T-junctions. A square metallic plate is inserted in both T-junctions to broaden the impedance matching bandwidth [26]. For the modified T-junction, the distances between the output ports are reduced to accommodate d_1. A stepped single-ridge waveguide working as a three-section impedance transformer is used to further increase the bandwidth. In addition, an inductive metallic post is loaded on the square metallic plate of the modified T-junction to enhance the isolation between the adjacent ports.

Finally, a transition structure is required from the external standard waveguide port (WR-28) to the single-ridge waveguide. As shown in Fig. 10, it is again a three-section wideband impedance transformer.

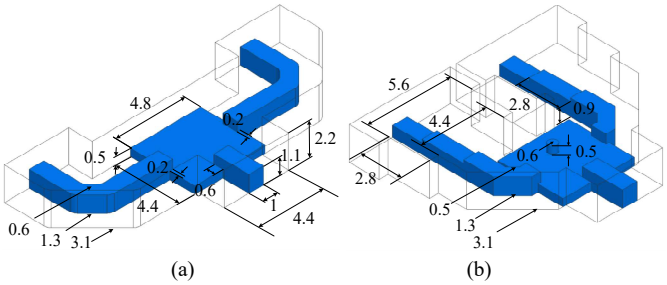

Fig. 9. Structure and dimensions: (a) Single-ridge T-junction; (b) Modified single-ridge T-junction.

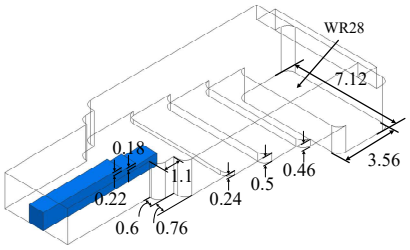

Fig. 10. Structure and dimensions of the feeding transition.

With the optimized dimensions of the single-ridge T-junction, the modified single-ridge T-junction and the transition (shown in Fig. 9 and 10), the feed network achieves S_{11} below -15 dB over the band of 26-42 GHz and a balanced transmission coefficient within -9 ± 0.2 dB across the eight output ports.

III. MEASUREMENTS AND DISCUSSION

For the convenience of manufacturing, the CTS FSA is divided into three parts (M1, M2 and M3, as illustrated in Fig. 1). All parts are fabricated out of aluminum by milling and assembled by means of screws. Fig. 11 shows the photographs of three separate blocks and the assembled FSA. The overall size of the CTS array is 133 mm × 93 mm × 21 mm. The radiation performances are measured using NSI near-field vertical planar scanner systems.

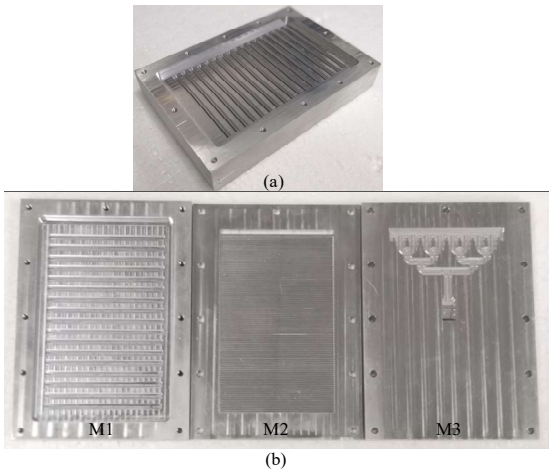

Fig. 11. Photographs of the fabricated CTS antenna array: (a) assembled antenna; (b) separated layers.

A. Reflection coefficient

The reflection coefficient is measured using Agilent E8361C. The simulated and measured reflection coefficients are shown in Fig. 12. Reasonably good agreement has been achieved. The matching is better than -12.5 dB over the frequency range of 26 - 42 GHz (47% fractional bandwidth).

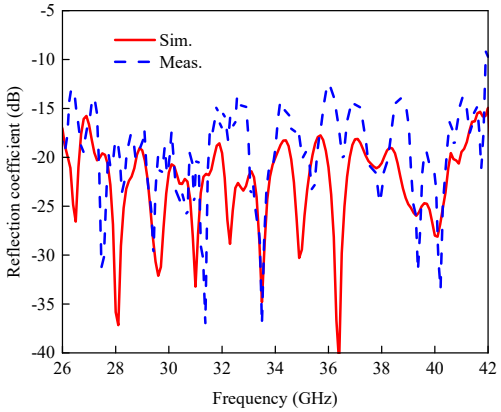

Fig. 12. Simulated and measured reflection coefficients.

B. Radiation patterns

The simulated and measured radiation patterns at a number of frequencies are plotted in Fig. 13. The measured side lobes are lower than -12.6 dB at all frequencies. To show the scanning capability, the simulated and measured main beam angles at different frequencies are given in Fig. 14. In simulation, this is from 0° to −50° with the frequency decreasing from 42 GHz to 26 GHz. The measured scanning range is from −2.2° to −56.2°. The small discrepancy is partly caused by the measured error and partly attributed to the imperfection in the fabrication and assembly. The slight changes of the slopes k_1 and k_2 generate phase errors and affect the main beam angles. It has been found of that a little change of the lower slope k_1

could cause a small angular offset. This is shown in Fig. 15. Indeed, the bottom of the trench and the lower slope in the slow-wave structure are subject to larger and more unpredictable fabrication errors during machining.

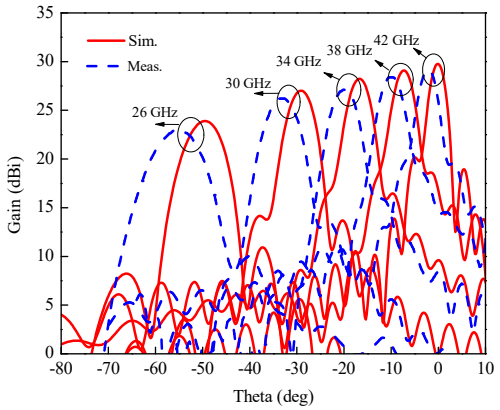

Fig. 13. Simulated and measured radiation patterns.

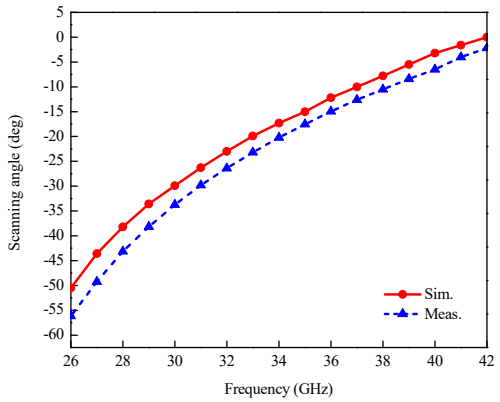

Fig. 14. Simulated and measured scanning angle against frequency.

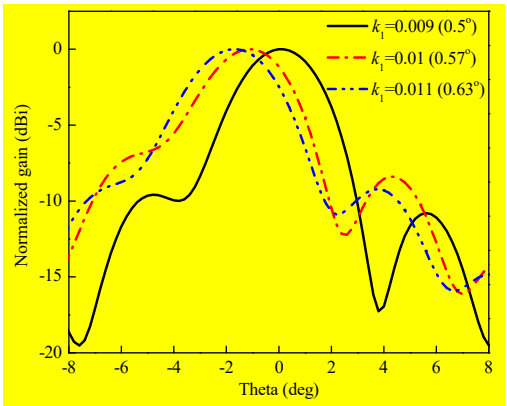

Fig. 15. Effect of k_1 on the scanning angles at 42 GHz.

C. Antenna peak gain

Fig. 16 compares the simulated and measured peak gain versus operating frequency. The simulated peak gain is in the range of 23.7 - 29.7 dBi between 26 and 42 GHz, whereas the measured peak gain is 22.9 - 29.2 dBi. The measured peak gain is slightly lower than the simulated. The small difference comes from two potential sources: fabrication tolerance and measurement error. The estimated aperture efficiency is between 52% and 71%, while the measured radiation efficiency is between 63% and 89 %. The power dissipation is believed to be mainly due to the imperfection from the multi-layered assembly and the conductor losses. The assembly of a multi-layer structure is often associated with excessive power loss due to poor conductive contacts. Unfortunately, this is difficult to quantify either in simulation or by experiment. The fine features in the slow-wave structure aggravate the conductor loss. Estimated by simulation, the conductor loss accounts for 0.5 dB. In addition, as expected the dispersion effect affects the radiation efficiency at large scanning angles.

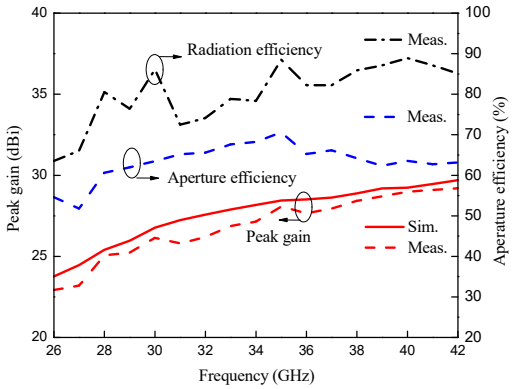

Fig. 16. Simulated and measured peak gain, radiation and aperture efficiency.

D. Comparison with other work

TABLE I
MEASURED RADIATION PERFORMANCE OF THE PROPOSED FSA

Freq. (GHz)	Scanning angle (°)	Peak gain (dBi)	1st side lobe (dB)	3-dB BW (°)	Aperture efficiency (%)
26	−56.2	22.9	−12.9	11.25	54.6
28	−43.1	25.1	−13.6	9.2	60.6
30	−33.8	26.2	−12.6	7.75	63.5
32	−26.4	26.2	−16	6.75	65.6
34	−20.2	27.1	−15.5	6	69.2
36	−14.9	27.7	−14.5	5.75	65.5
38	−10.5	28.4	−13.9	5.5	64.2
40	−5.9	29	−13	5	63.5
42	−2.2	29.2	−14	4.25	63.2

TABLE II
PERFORMANCE COMPARISON OF FREQUENCY-SCANNED ANTENNA ARRAYS

Ref.	Type	Bandwidth (GHz)	Scanning angle (°)	Radiation efficiency	Peak gain (dBi)
[14]	SW	240~315	−30~30	35%	19~22.5
[15]	SW	87~102	−5~25	70%	8~16
[18]	CPW-CTS	2.24~2.63	58~124	N/A	11
[19]	SIW-CTS	8.5~14.1	52.2~−16.8	N/A	15.1~18.1
[20]	SIW-CTS	27.06~36	−43~3	67%	12.8 ~17.8
This work	WG-CTS	26~42	−56.2~−2.2	>63%	22.9~29.2

The measured radiation performance of the FSA at different operating frequencies is summarized in Table I. The table gives peak gain, scanning angle (main beam angle), level of the 1st side lobe, 3-dB beam width (BW) and aperture efficiency. Table II compares the performance of this design with several other published FSAs. Among them, [18] utilized a CPW-feed CTS structure. Due to the relatively high loss of planar transmission lines, it may not be

suitable for MMW applications. Other designs are based on SW or SIW CTS structures. With its wideband LSG and non-uniform slow-wave structure, the proposed waveguide FSA offers the highest gain, the largest fractional bandwidth and has a comparable scanning angle, while maintaining very competitive radiation performance overall.

IV. Conclusions

In this paper, a waveguide-based wideband CTS FSA has been demonstrated. A novel LSG constructed of a PPW with multiple-port excitation is introduced to generate the quasi-TEM wave. By adjusting the non-uniform slow-wave structure underneath the CTS radiation slots, the amplitude and phase distribution of the quasi-TEM wave at the radiation slots can be controlled and optimized. An experimental prototype with the broad operation band of 26 to 42 GHz was designed and implemented. Experimental results show that the proposed FSA has a wide scanning angle from -56.2° to -2.2° with peak gains between 22.9 and 29.2 dBi. Compared with the previous work, the proposed CTS FSA shows a wider impedance bandwidth and scanning angle while maintaining a competitive radiation performance. It has demonstrated very attractive performance and great potentials for millimeter-wave applications.

References

[1] F. Siaka, M. A. Tehrani, J. J. Laurin and Y. Savaria, "Radar system with enhanced angular resolution based on a novel frequency scanning reflector antenna," *IET Radar, Sonar & Navigation*, vol. 11, no. 2, pp. 350-358, Feb. 2017.

[2] M. R. Naeini, M. Fakharzadeh and F. Farzaneh, "Travelling-wave Ka-band frequency scanning antennas for millimeter-wave imaging applications," in *International Symposium on Telecommunications (IST)*, Tehran, 2016, pp. 591-595.

[3] J. Huang, W. Lin, F. Qiu, C. Jiang, D. Lei and Y. J. Guo, "A low profile, ultra-lightweight, high efficient circularly-polarized antenna array for Ku band satellite applications," *IEEE Access*, vol. 5, pp. 18356-18365, 2017.

[4] H. Bayer, A. Krauss, T. Zaiczek, R. Stephan, O. Enge-Rosenblatt and M. A. Hein, "Ka-band user terminal antennas for satellite communications," *IEEE Trans. Antennas Propag*., vol. 58, no. 1, pp. 76-88, Feb. 2016.

[5] M. Ettorre, F. F. Manzillo, M. Casaletti, R. Sauleau, L. L. Coq and N. Capet, "Continuous transverse stub array for Ka-band applications," *IEEE Trans. Antennas Propag.*, vol. 63, no. 11, pp. 4792-4800, Nov. 2015.

[6] X. Lu, S. Gu, X. Wang, H. Liu and W. Lu, "Beam-scanning continuous transverse stub antenna fed by a ridged waveguide slot array," *IEEE Antennas Wireless Prop. Lett.,* vol. 16, pp. 1675-1678, 2017.

[7] G. B. Wu, S. W. Qu and C. H. Chan, "Wide-angle beam scanning reflect array antenna design using phase matching method," in *Global Symposium on Millimeter-Waves (GSMM)*, Hong Kong, 2017, pp. 132-133.

[8] H. Bolandhemmat, M. Fakharzadeh, P. Mousavi, S. H. Jamali, G. Z. Rafi and S. Safavi-Naeini, "Active stabilization of vehicle-mounted phased-array antennas," *IEEE Trans. Veh. Technol.*, vol. 58, no. 6, pp. 2638-2650, July. 2009.

[9] F. Tiezzi, D. Llorens, C. Dominguez and M. Fajardo, "A compact Ku-band transmit/receive low-profile antenna for broadband mobile satellite communications," in *Proc. European Conference on Antennas and Propagation (EuCAP)*, Barcelona, Spain, 2010, pp. 1-4.

[10] M. Alibakhshi-Kenari, A. Andújar, and J. Anguera, "New compact printed leaky-wave antenna with beam steering," *Microw. Opt. Technol. Lett*, vol. 58, no. 1, pp. 215–217, 2016.

[11] K. Ren and Y.Q. Fu, "A K-band frequency scanning microstrip array using SIW," in *IEEE International Conference on Microwave and Millimeter Wave Technology (ICMMT)*, Beijing, 2016, pp. 452-454.

[12] Y. J. Cheng, W. Hong and K. Wu, "Millimeter-wave substrate integrated waveguide multibeam antenna based on the parabolic reflector principle," *IEEE Trans. Antennas Propag.*, vol. 56, no. 9, pp. 3055-3058, Sept. 2008.

[13] F. Paredes, G. Zamora, S. Zufanelli, F. J. Herraiz-Martínez, J. Bonache, and F. Martín, "Recent advances in multiband printed antennas based on metamaterial loading," *Advances in OptoElectronics*, vol. 2012, Article ID 968780, 12 pages, 2012.

[14] R. Camblor, S. V. Hoeye, M. Fernández, C. Vázquez Antuña and F. Las-Heras, "Submillimeter wavelength 2-D frequency scanning antenna based on slotted waveguides fed through a phase shifting network," *IEEE Trans. Antennas Propag.*, vol. 65, no. 7, pp. 3501-3509, July 2017.

[15] L. Ranzani, E. D. Cullens, D. Kuester, K. J. Vanhille, E. Grossman and Z. Popović, "W-band micro-fabricated coaxially-fed frequency scanned slot arrays," *IEEE Trans. Antennas Propag*., vol. 61, no. 4, pp. 2324-2328, April 2013.

[16] W. W. Milroy, "The continuous transverse stub (CTS) array: basic theory, experiment, and application," *Proc. Antenna Appl*. Symp., Sep. 25–27, 1991, vol. 2, pp. 253–283.

[17] Y. Xu, H. Dong, Y. Liu and P. Zhang, "Continuous transverse stub (CTS) array antenna," in *Int. Symp. Antennas Propag. (ISAP)*, 2012, pp. 1083–1086.

[18] Y. Li, M. F. Iskander, Z. Zhang and Z. Feng, "A new low cost leaky wave coplanar waveguide continuous transverse stub antenna array using metamaterial-based phase shifters for beam steering," *IEEE Trans. Antennas Propag*., vol. 61, no. 7, pp. 3511-3518, July. 2013.

[19] X. X. Yang, L. Di, Y. Yu and S. Gao, "Low-profile frequency-scanned antenna based on substrate integrated waveguide," *IEEE Trans. Antennas Propag*., vol. 65, no. 4, pp. 2051-2056, April 2017.

[20] H. Choe and S. Lim, "Millimeter-wave continuous transverse stub (CTS) antenna array using substrate integrated waveguide (SIW) technology," *IEEE Trans. Antennas Propag*., vol. 62, no. 11, pp. 5497–5503, Nov. 2014.

[21] F. F. Manzillo, M. Ettorre, M. Casaletti, N. Capet and R. Sauleau, "Active impedance of infinite parallel-fed continuous transverse stub arrays," *IEEE Trans. Antennas Propag.*, vol. 63, no. 7, pp. 3291-3297, July. 2015.

[22] W. W. Milroy, "Planar antenna radiating structure having quasi-scan frequency independent driving point impedance," US Patent 5,995,055, Nov. 1999.

[23] K. Tekkouk, J. Hirokawa, R. Sauleau and M. Ando, "Wideband and large coverage continuous beam steering antenna in the 60-GHz band," *IEEE Trans. Antennas Propag.*, vol. 65, no. 9, pp. 4418-4426, Sept. 2017.

[24] J. Gao , X. Lei , G. Chen, Y. Zhang and J. Wu, "Design of the variable inclination continuous transverse stub antenna based on rectangular grating slow-wave structure," *Int. J. Antenn. Propag*, vol. 2018, Apr. 2018.

[25] M. Samardzija, T. Kai, J. Hirokawa and M. Ando, "Single-layer waveguide feed for uniform plane TEM-wave in oversized-rectangular waveguide with hard-surface sidewalls," *IEEE Trans. Antennas Propag.*, vol. 54, no. 10, pp. 2813-2819, Oct. 2006.

[26] Q. X. Chu, Z. Y. Kang, Q. S. Wu and D. Y. Mo, "An in-phase output Ka-band traveling-wave power divider/combiner using double ridge-waveguide couplers," *IEEE Trans. Microw. Theory Techn.*, vol. 61, no. 9, pp. 3247-3253, Sept. 2013.